Available online at www.sciencedirect.com
ScienceDirect
Trans. Nonferrous Met. Soc. China 30(2020) 1452−1462
Transactions of Nonferrous Metals Society of China
www.tnmsc.cn

Near-net shaped Al/SiC_P composites via vacuum-pressure infiltration combined with gelcasting

Cui-ge DONG[1,2], Ri-chu WANG[1,2], Yi-xin CHEN[1,2], Xiao-feng WANG[1,2], Chao-qun PENG[1], Jing ZENG[1,2]

1. School of Materials Science and Engineering, Central South University, Changsha 410083, China;
2. Hunan Provincial Key Laboratory of Electronic Packaging and Advanced Functional Materials, Changsha 410083, China

Received 14 November 2019; accepted 30 April 2020

Abstract: To solve the problem of difficult machining, the near-net shaped Al/SiC_P composites with high volume fraction of SiC particles were fabricated by vacuum-pressure infiltration. The SiC_P preform with a complex shape was prepared by gelcasting. Pure Al, Al4Mg, and Al4Mg2Si were used as the matrices, respectively. The results indicate that the optimal parameters of SiC_P suspension in gelcasting process are pH value of 10, TMAH content of 0.5 wt.%, and solid loading of 52 vol.%. The Al matrix alloyed with Mg contributes to improving the interfacial wettability of the matrix and SiC particles, which increases the relative density of the composite. The Al matrix alloyed with Si is beneficial to inhibiting the formation of the detrimental Al_4C_3 phases. The Al4Mg2Si/SiC_P composite exhibits high relative density of 99.2%, good thermal conductivity of 150 $W\cdot m^{-1}\cdot K^{-1}$, low coefficient of thermal expansion of 10.1×10^{-6} K^{-1}, and excellent bending strength of 489 MPa.

Key words: Al/SiC_P composites; gelcasting; vacuum-pressure infiltration; microstructure; properties

1 Introduction

Al/SiC_P composite with high fraction of SiC particles is an advanced electronic packaging material in thermal management applications due to its high thermal conductivity (TC), low coefficient of thermal expansion (CTE), good mechanical properties and low density [1−3]. The inter-connected Al matrix provides an effective heat transfer channel, and the low expansion SiC particles can restrain the heat distortion of the matrix and enhance the soft Al. Considering the combination of the advantages of both Al and SiC_P, the Al/SiC_P composite with high fraction of SiC_P has attracted considerable interests from many researchers, and the homogeneous distribution of SiC particles and the cohesion of particle−matrix interface are their most concerned problems [4−6].

For the poor dispersion of the high volume fraction (more than 50%) SiC particles in the Al matrix, it is difficult to obtain high-performance Al/SiC_P composite by conventional stir casting method [7−9]. Besides, the prepared composite is difficult to be machined into complex component owing to the large number of high-hardness SiC particles. Fortunately, the melt infiltration combined with net shape technology may be a promising method to fabricate high-performance Al/SiC_P composite with a complex shape, and can also reduce subsequent processing procedures effectively [10]. In the melt infiltration method, it is needed to prepare the 3D-SiC preform firstly, and then the molten Al alloy is infiltrated into the

Foundation item: Project (CXZZ20140506150310438) supported by the Science and Technology Program of Shenzhen City, China; Project (2017GK2261) supported by the Science and Technology Program of Hunan Province, China; Project (2017zzts111) supported by the Fundamental Research Funds for the Central Universities, China

Corresponding author: Jing ZENG; Tel: +86-15116335400; E-mail: zengjing@csu.edu.cn

DOI: 10.1016/S1003-6326(20)65310-9

preform by pressure or pressureless infiltration process [11−14]. For the first step, gelcasting is a promising technique for complex shaping of structural ceramics. Compared with conventional mould forming [12] and tape casting [15], the outstanding advantage of the technique is that the suspension can be in situ consolidated [16], which results in near-net-shape forming without subsequent machining. For the second step, compared with pressure infiltration, the melting alloy cannot completely fill the network preform when infiltrated by pressureless infiltration, resulting in preparation defects, and a higher infiltration temperature is needed to ensure the melt fluidity [5]. It is known that the brittle and harmful Al_4C_3 phases are inevitably formed near the Al/SiC_P interface at 650−1000 °C, and a higher infiltration temperature means that more Al_4C_3 phases will precipitate, which is detrimental to the thermal conductivity and mechanical properties of the composite [5,7].

Furthermore, some alloying elements play an important role in alleviating the detrimental interfacial reaction and provide good wettability between SiC particles and Al matrix, which contributes to obtain high-performance Al/SiC_P composite [17]. It is pointed out that the Al matrix alloyed with Si can improve the Si activity in the solution and inhibit the detrimental reaction at SiC_P/Al interface in a thermodynamic way, as depicted in following reaction [18,19]:

$$4Al(l)+3SiC(s)=Al_4C_3(s)+3Si(s) \quad (1)$$

Besides, both Si and Mg additions to Al matrix can improve the infiltration rate and help to produce a pore-free composite [13]. Additionally, Mg element can provide a good interfacial wetting and enhance the interfacial bonding by disrupting the oxide films at the Al drop and SiC surfaces, as evidenced from the following reactions [4,20]:

$$2SiO_2+2Al+5Mg=MgAl_2O_4+2Mg_2Si \quad (2)$$

$$4Mg+SiO_2=2MgO+Mg_2Si \quad (3)$$

$$4Al+3SiO_2=2Al_2O_3+3Si \quad (4)$$

In this work, to solve the problem of difficult machining of the hard composites, near-net shaped Al/SiC_P composites with a uniform distribution of ceramic particles were fabricated through a gelcasting method followed by a vacuum-pressure infiltration process. The effects of pH value, dispersant content and solid loading on the rheological properties of SiC_P suspension were investigated. Besides, the effects of Mg and Si additions on the microstructure and properties of the composites were evaluated.

2 Experimental

2.1 Materials

The matrices were pure Al with a purity of 99.99%, self-made Al−4wt.%Mg alloy (Al4Mg), and Al−4wt.%Mg−2wt.%Si alloy (Al4Mg2Si). The commercial green SiC powders with two different sizes (51 and 4 μm) were used, and the optimum mass ratio of the coarse and fine powders are 2:1 according to our previous literature [14]. The BET surface areas of two kinds of powders are 0.151 and 2.460 m^2/g, respectively. Acrylamide (AM), *N*,*N*′-methylenebisacrylamide (MBAM), and tetramethyl ammonium hydroxide (TMAH) were used as the monomer, cross linker, and dispersant, respectively. Ammonium persulfate (APS) and *N*,*N*,*N*′,*N*′-tetramethylenediamine (TEMED) were applied as the redox initiator pair for the gelcasting process.

2.2 Preparation of Al/SiC_P composites with complex shape

The schematic diagram for preparation process of Al/SiC_P composites is illustrated in Fig. 1. First, the monomer and crosslinking agent were dissolved into the distilled water to form homogeneous solution. Then, SiC powders were added into the solution, and the suspensions of 48−52 vol.% solid loading were ball-milled in WC cans by conducting on a planetary ball mill at 150 r/min for 24 h. The mass ratio of SiC powders to Al_2O_3 balls with diameter of 3−8 mm was 1:15. Second, the binder and initiators were added into the suspension by continuous stirring. Then, the suspension was cast into a graphite mould, and consolidated at 60 °C for 2 h. The macrographs of graphite moulds with different shapes are displayed in Fig. 2. Third, the SiC_P preform and graphite mould were put into the vacuum-pressure infiltration furnace, then vacuumed and heated to 670 °C. The molten alloy of about 700 °C covered the outer surface of the preform. Next, the high-pressure argon was injected into the furnace with the sustained pressure of 4 MPa, and the molten alloy was squeezed into the

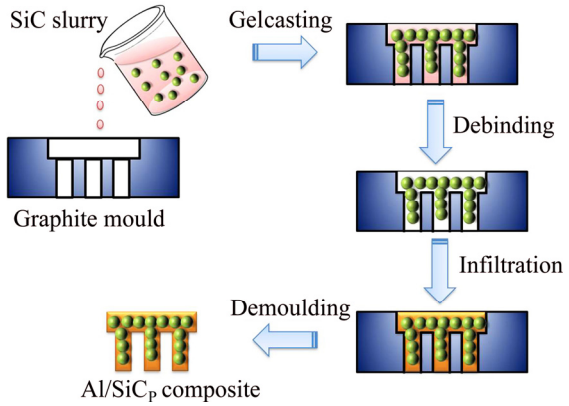

Fig. 1 Schematic diagram for preparation process of Al/SiC_P composites

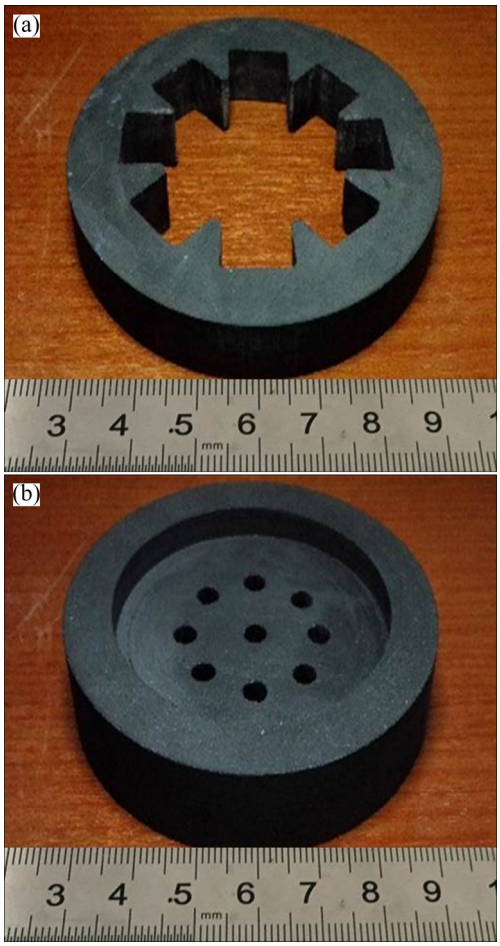

Fig. 2 Macrographs of graphite moulds with different shapes

preform with the help of the pressure difference outside and inside the preform. Three matrices (pure Al, Al4Mg and Al4Mg2Si) were used to prepare the composites. After vacuum pressure infiltration, Al/SiC_P composites with different shapes were removed from the graphite mould.

2.3 Characterization

Zeta potentials of the SiC powders were measured by Zeta potential analyzer (Zetasizer 4, Malvern Instruments Ltd.). The rheological measurements were performed on a rheometer (AR 2000, TA Instrument). The microstructures were characterized with an optical microscope (OM, XJP−6A) and a scanning electron microscope (SEM, FEI QUANTA−200). The elemental distributions of the composite were studied by electron probe microanalysis (EPMA, JXA−8230). The transmission electron microscopy (TEM) analyses used a Titan G2 60-300 equipped with EDS detector. Samples for TEM observation were mechanically thinned to 50−80 μm, followed by dimpling and ion-milling. Three-point bending strength was measured with a span of 30 mm and a cross-head speed of 0.5 mm/min, using CSS−44100 universal testing machine. Samples for three-point bending test with the dimension of 4 mm × 3 mm × 40 mm were cut from the composites. The density of the composite was tested by Archimedes method. The thermal diffusivity and specific heat capacity were tested using laser flash techniques and calorimetric methods (NETZSCH LFA427/3/G), respectively, and these tests were carried out on the cylindrical samples with the dimension of *d*10 mm × 3 mm. The thermal conductivity (TC) was the product of thermal diffusivity, specific heat capacity and density. The coefficient of thermal expansion (CTE) was measured on a NETZSCH DIL 402C dilatometer. The dimension of the samples for CTE test was *d*5 mm × 25 mm.

3 Results and discussion

3.1 Zeta potentials

The Zeta potentials of SiC powder dispersed in the organic monomer solutions with TMAH as dispersant are shown in Fig. 3. The isoelectric point (IEP) of SiC_P in deionized water with TMAH is pH_{iep}=4. When the pH value is 8−12, the absolute value of Zeta potential of SiC_P suspension is larger, which indicates that SiC_P suspension has good dispersion. According to DLVO theory and steric stability theory [21], higher Zeta potential is necessary for stable and low viscosity slurry. Furthermore, considering the corrosion of the suspension in the subsequent gelcasting process, pH value of the suspensions is chosen to be 10.

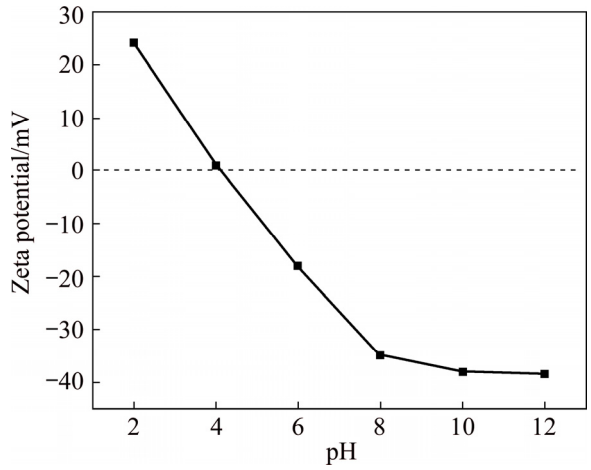

Fig. 3 Zeta potential of SiC_P as function of pH with dispersant of TMAH

3.2 Rheological properties

The rheological properties of SiC_P suspensions rely not only on pH values, but also on the dispersant content and solid loading. Figure 4 shows the effect of dispersant content on the viscosity of SiC_P suspensions with a solid loading of 50 vol.%. The viscosities of all suspensions decrease first and then increase with the increase of shear rate, indicating the shear thinning and shear thickening behavior. When the TMAH content of SiC_P suspension is 0.5 wt.%, its viscosity is much less than the suspension with 0.25 wt.% TMAH. While the TMAH content increases to 0.5−1.0 wt.%, larger dispersant content corresponds to higher viscosity. TMAH, a small molecule dispersant, improves the stability of the suspension by electrostatic repulsion force instead of steric hindrance effect [22]. In aqueous dispersion, organic cation (TMA^+) is combined with free silanol or siloxane on the surface of SiC_P to increase the thickness of the stern double layer, thus improving the electrostatic repulsion force and reducing the viscosity [15]. However, further improvement of TMAH will increase the viscosity of suspensions [23]. In detail, excess TMAH as free electrolyte will increase the ionic strength of the suspension and interfere with the electrostatic repulsion force among SiC particles. In addition, it will generate partial bridging of dispersed SiC_P and result in slight flocculation of the suspension.

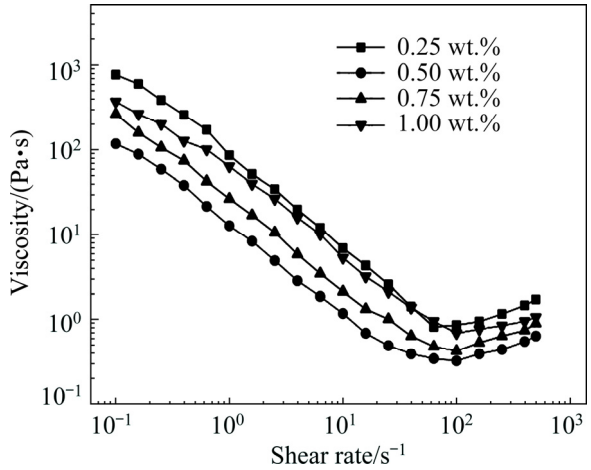

Fig. 4 Rheological properties of SiC_P suspensions with different TMAH contents

The solid loading of the starting suspension is one of the critical issues for the gelcasting process that should be well controlled. The effect of the solid loading on the viscosity of SiC_P suspension with 0.5 wt.% TMAH is shown in Fig. 5. When the solid loading is 48−52 vol.%, the suspension has a good rheological property. While the solid loading reaches 54 vol.%, the viscosity of SiC_P suspension increases rapidly when the shear rate is higher than 1 s^{-1}, showing a shear thickening behavior. Therefore, the SiC_P suspension with solid loading over 54 vol.% is unstable and easy to deposit, which is unsuitable for gelcasting.

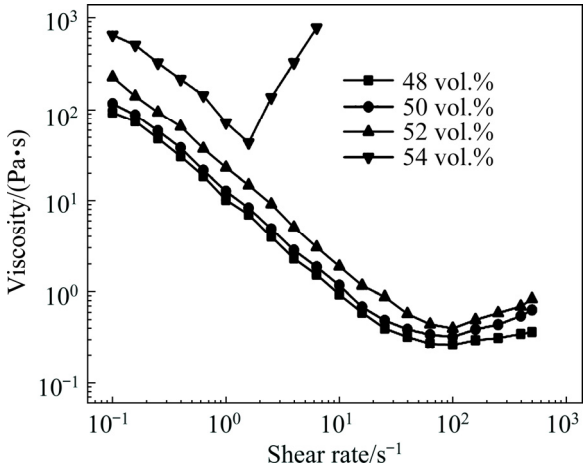

Fig. 5 Rheological properties of SiC_P suspensions with different solid loadings

A low viscosity is needed for preparing SiC_P preform by gelcasting method, and high solid loading is required by Al/SiC_P composites for electronic packaging. Thus, SiC_P suspension with a pH value of 10, a TMAH content of 0.5 wt.% and a solid loading of 52 vol.% were configured and applied in the gelcasting process.

3.3 Microstructures and properties of Al/SiC_P composites with complex shape

Due to the excellent rheological properties of the suspensions, the complex SiC_P preforms can be successfully prepared, and the macrographs are illustrated in Figs. 6(a, b). The Al/SiC_P composites prepared based on the SiC_P preforms are presented in Figs. 6(c, d). A small amount of Al layer on the surface of the composites has been polished and removed. It is clear that Al fluid can effectively penetrate the SiC_P preforms to obtain the Al/SiC_P composites and maintain their morphologies after the vacuum pressure infiltration process to realize near-net shape forming without any machining process.

Table 1 presents the relative density, thermal conductivity, coefficient of thermal expansion, and three-point bending strength of the composites with three different matrices. It is clear that the composite with the pure Al matrix has the worst thermal properties and mechanical properties, which results from the low relative density of 91.1%. In comparison, the composites with the Al4Mg and Al4Mg2Si matrices have a better comprehensive performance, which mainly attributes to the higher relative density after adding a few amounts of Mg and Si elements. Noticeably, a good combination of high strength (489 MPa) and high thermal conductivity (150 $W \cdot m^{-1} \cdot K^{-1}$) is achieved in the Al4Mg2Si/SiC_P composite.

Figure 7 depicts the metallographic microstructures of the composites. The SiC particles are homogeneously distributed throughout the Al matrix, and the small-sized SiC particles fill into the free space left by the large-sized SiC particles. The black areas in the images indicate pores produced

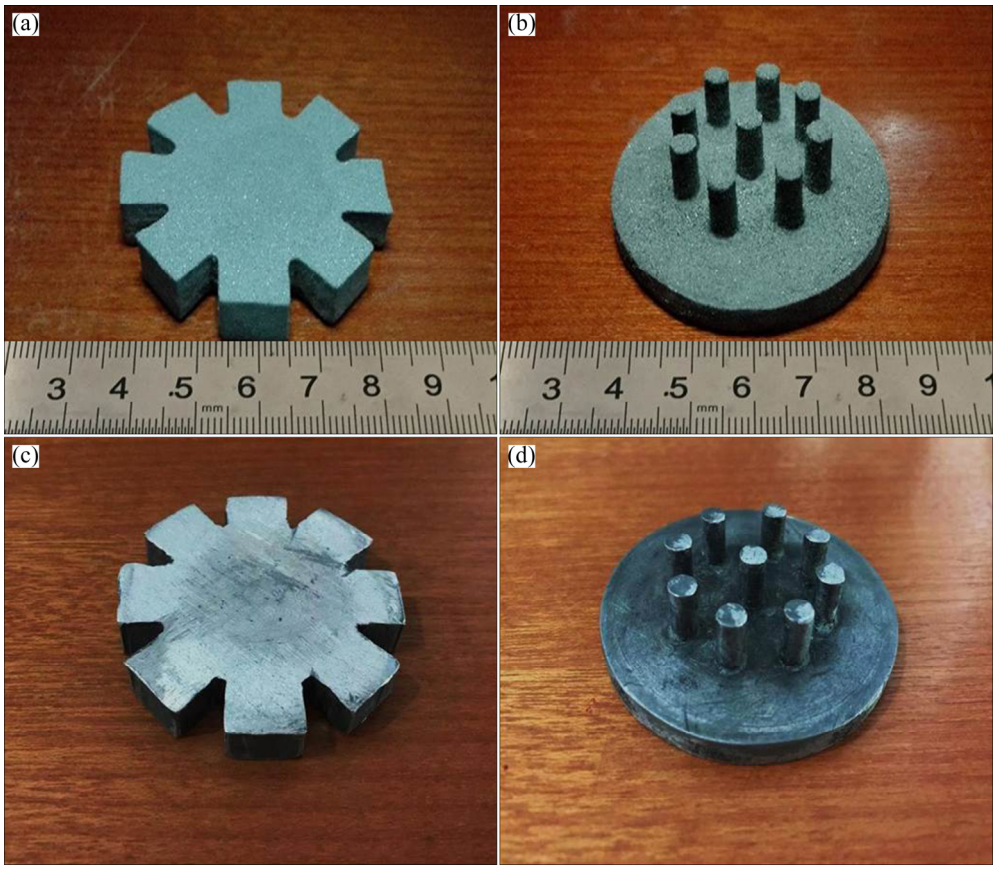

Fig. 6 Macrographs of SiC_P performs (a, b) and Al/SiC_P composites (c, d)

Table 1 Properties of composites with three different matrices

Composite	TC/($W \cdot m^{-1} \cdot K^{-1}$)	CTE/10^{-6} K^{-1}	Strength/MPa	Relative density/%
Al/SiC_P	132	10.9	386	91.1
Al4Mg/SiC_P	151	10.2	461	97.9
Al4Mg2Si/SiC_P	150	10.1	489	99.2

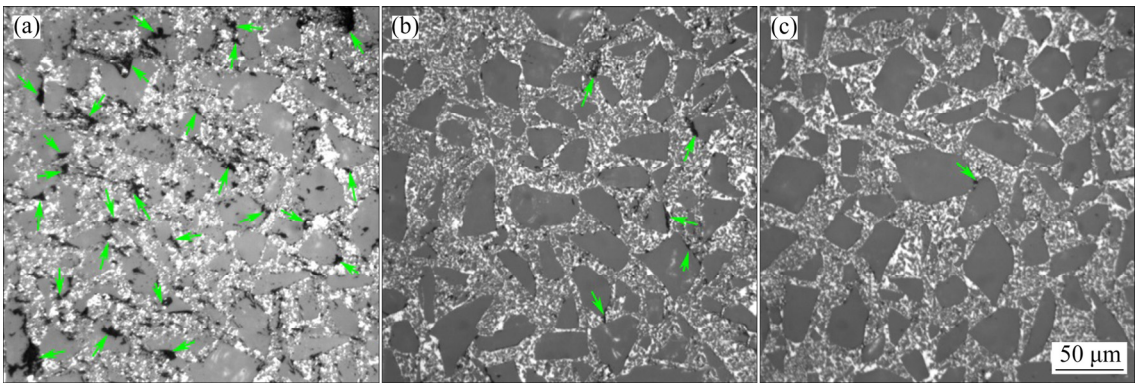

Fig. 7 OM images of Al/SiC_P (a), Al4Mg/SiC_P (b), and Al4Mg2Si/SiC_P (c) composites

during infiltration. A large number of pores are noticed in the composite with the pure Al matrix (Fig. 7(a)). The number of pores is greatly reduced when the matrix is alloyed with 4 wt.% Mg (Fig. 7(b)). It is worth mentioning that few pores are observed in the composite with the combined addition of 4 wt.% Mg and 2 wt.% Si (Fig. 7(c)), and a high relative density of 99.2% is obtained. This means that the alloyed matrix improves the relative density of the composite significantly.

In the process of vacuum-pressure infiltration, a higher infiltration temperature contributes to higher melt flow rate and lower melt viscosity, thus leading to a denser composite. However, the reported studies suggest that the interface product, Al_4C_3, can be formed at the SiC_P/Al interface when the infiltration temperature is 650−1000 °C, and a higher infiltration temperature means more detrimental Al_4C_3 phases in the composite [5,11,20]. As aforementioned, 700 °C is chosen as infiltration temperature to reduce the formation of interface product Al_4C_3 to the maximum extent and guarantee a satisfactory melt fluidity simultaneously. The pure Al matrix is not suited to prepare the composite due to its poor melt fluidity at 700 °C, which leads to the formation of many pores at the interface, as depicted in Fig. 7(a). The infiltration rate is faster and the infiltration will become much easier when the matrix is alloyed with Mg and Si [13,20].

Figure 8 illustrates the SEM microstructure and corresponding elemental distribution maps of the Al4Mg2Si/SiC_P composite. It can be seen that the Si element mainly exists in the SiC particles, and there is no obvious interfacial reaction between matrix and SiC particles. In addition, small amounts of Mg and Si elements distribute in the matrix in the form of solid solution. On one hand, the addition of Si restrains the reaction of Al and SiC_P, thus reducing the formation of Al_4C_3 phases [19]. On the other hand, alloying of Al with Mg reduces the Al surface tension and the Al/SiC_P interfacial free energy, and improves the wettability of interface by breaking the thin oxide layers on the surface of the SiC particles [20].

Figure 9 presents the TEM images of the composite with matrix of pure Al and the EDS analysis of Al_4C_3 phases. Fine SiC particles are uniformly distributed into the matrix (Fig. 9(a)), but some voids can be observed at the interface between Al matrix and SiC particles (Fig. 9(b)). When the melt is infiltrated at 700 °C, the molten pure Al exhibits relatively poor fluidity compared with the Si and Mg alloyed melt. Furthermore, the oxide layer on both SiC_P and Al drop surfaces hinders the direct contact between SiC particles and Al drops. It is the above two reasons that make voids at the interface inevitably occur in the Al/SiC_P composite when infiltrated at 700 °C. In addition, some precipitates in the shape of strip are observed at the Al/SiC_P interface (Fig. 9(c)), and the corresponding EDS analysis (Fig. 9(d)) indicates that they are Al_4C_3 phases.

TEM images of Al4Mg/SiC_P and Al4Mg2Si/SiC_P composites are illustrated in Figs. 10(a−f). The EDS results for Al4Mg/SiC_P composites from the marked regions in Figs. 10(a, b) are displayed in Figs. 10(g−i). After alloying with 4 wt.% Mg, the interface between SiC_P and Al in the composite is clean and continuous, and few voids are observed in Fig. 10(a). This means that Mg can improve the interfacial wettability effectively. It is noted that there are small amounts of Mg solutes in the Al

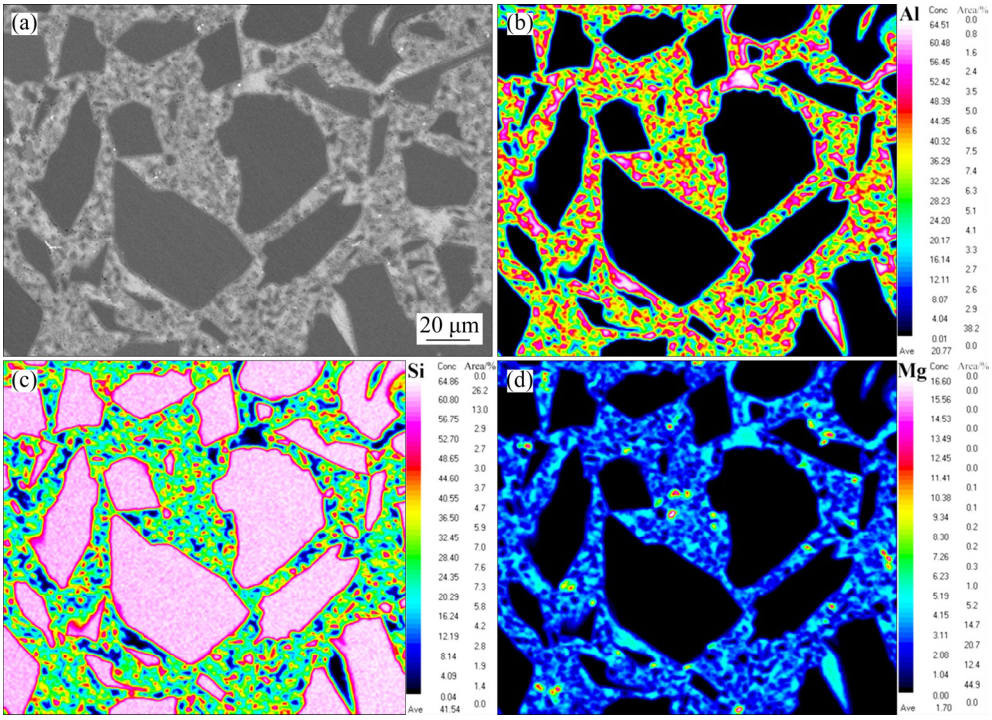

Fig. 8 Back-scattered electron image of Al4Mg2Si/SiC_P composite (a), and corresponding elemental distribution maps by EPMA: (b) Al; (c) Si; (d) Mg

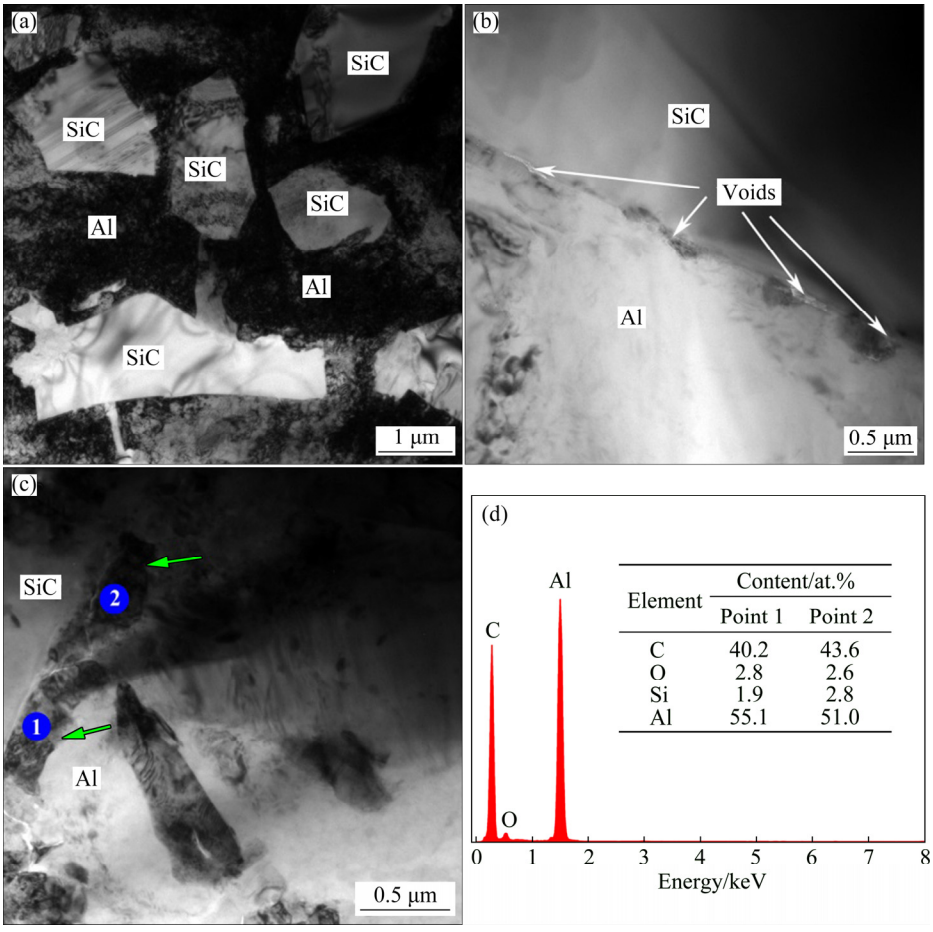

Element	Content/at.%	
	Point 1	Point 2
C	40.2	43.6
O	2.8	2.6
Si	1.9	2.8
Al	55.1	51.0

Fig. 9 TEM micrographs of Al/SiC_P composite (a−c) and EDS analysis of Al_4C_3 phase (d)

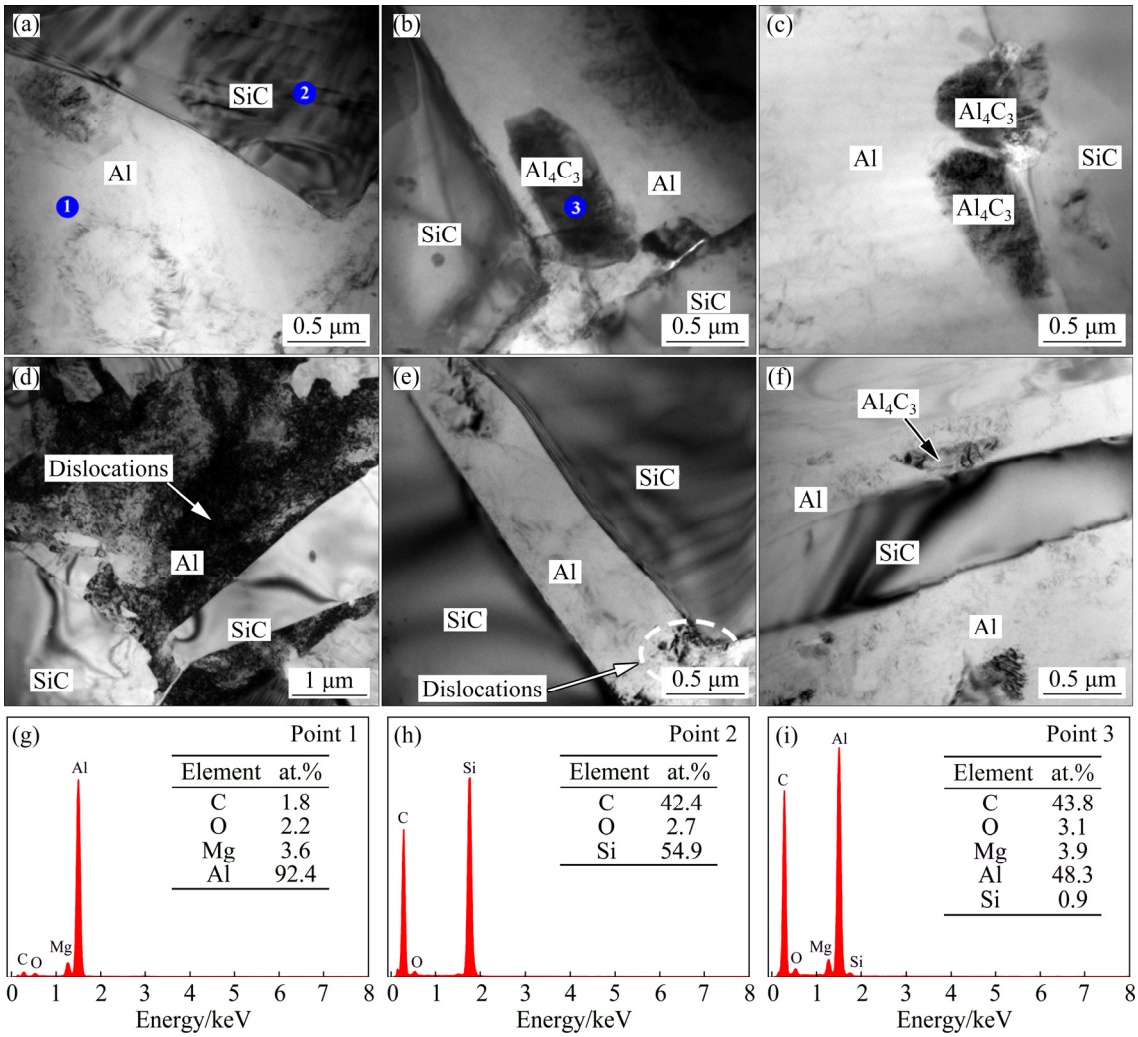

Fig. 10 TEM micrographs of Al4Mg/SiC_P composite (a−c), Al4Mg2Si/SiC_P (d−f) composite, and corresponding EDS spectra (g−i)

matrix, which exerts a solution strengthening effect on the soft matrix. However, deleterious Al_4C_3 phases are still observed near the Al/SiC_P interface in the Al4Mg/SiC_P composite (Fig. 10(b)), and some Al_4C_3 phases even corrode the Al/SiC_P interface and break the interfacial continuity (Fig. 10(c)). After adding 2 wt.% Si into the Al4Mg/SiC_P composite, both the size and number of Al_4C_3 phases decrease significantly, although a few Al_4C_3 phases can still be seen in Fig. 10(f). This means that a better adhesion at the Al/SiC_P interface is achieved. Consequently, this is verified by the fact that Si can effectively suppress the formation of deleterious Al_4C_3 phases. Besides, high density dislocations (Fig. 10(d)) are observed in the Al4Mg2Si/SiC_P composite due to the mismatch of the CTE between the matrix and SiC_P [24]. The retained dislocations also indicate the enhanced strength of the alloyed matrix, which is in conformity with the high strength of Al4Mg2Si/SiC_P composite. In addition, some dislocations in the Al matrix are distributed at the edge of the SiC particle (indicated by arrow in Fig. 10(e)), which means that micro-voids and cracks preferentially nucleate near the edge during failure process due to a relatively high stress concentration in this place.

The morphology of a typical ductile and brittle mixed fracture surface is observed in the Al4Mg/SiC_P and Al4Mg2Si/SiC_P composites, as depicted in Fig. 11. The hard SiC particles with two sizes are the main strengthening factors. The high fraction of SiC particles leads to a relatively flat fracture surface (Figs. 11(a, d)) and these particles are surrounded by the Al matrix with a large number of shallow and fine dimples (indicated by

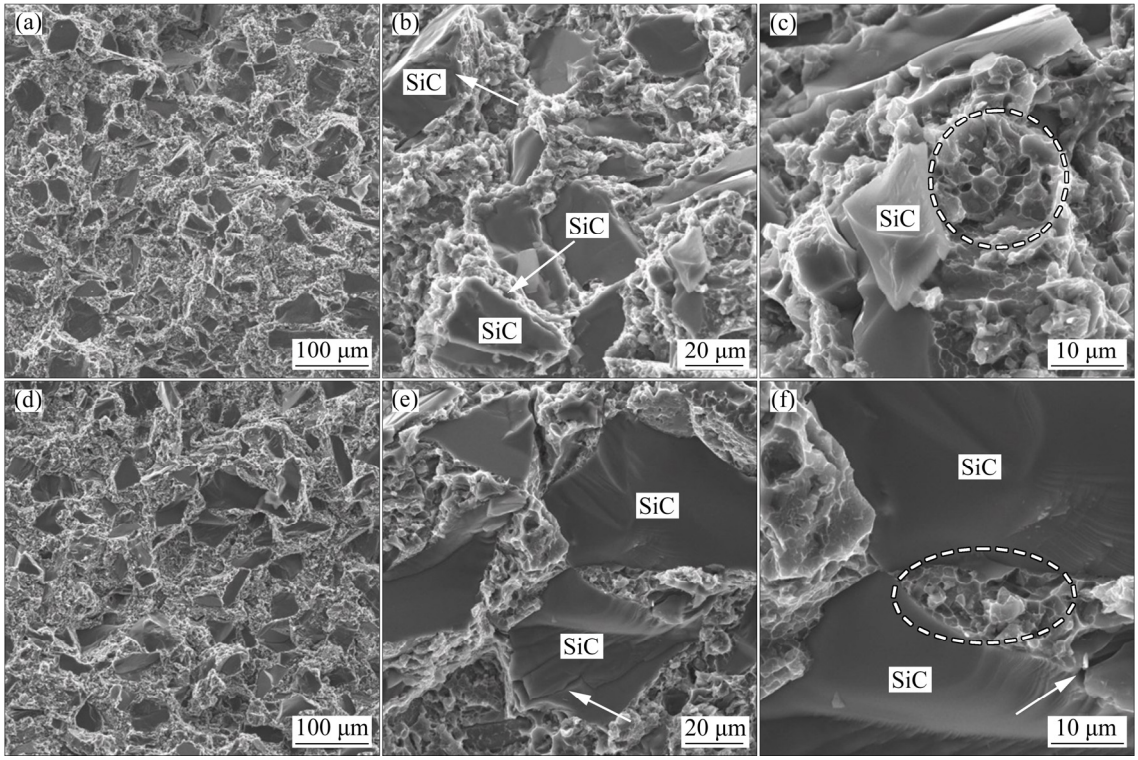

Fig. 11 Fractographs of Al4Mg/SiC_P (a−c) and Al4Mg2Si/SiC_P (d−e) composites

circles in Figs. 11(c, f)), which means a high strength but a poor ductility of the composites. In the Al4Mg/SiC_P composite, most of the SiC particles are brittle fractured, but a few particles are pulled out during three-point bending test, as indicated by the arrows in Fig. 11(b). The pullout of these particles indicates some weak Al/SiC_P interface caused by the deleterious Al_4C_3 phases. In comparison, few SiC particles are pulled out from the matrix in the Al4Mg2Si/SiC_P composite, which means an enhanced interfacial bonding between the matrix and SiC particles. The formation of Al_4C_3 is suppressed effectively by adding 2 wt.% Si into the matrix, which leads to a higher strength of the Al4Mg2Si/SiC_P composite. Additionally, the cracks in some SiC particles (as indicted by arrows in Figs. 11(e, f)) also suggest that these hard particles need to undergo much stronger stresses before fracture.

4 Conclusions

(1) To avoid machining the hard composites, a simple gelcasting method followed by a vacuum-pressure infiltration was utilized to prepare Al/SiC_P composites with a complex shape.

(2) The optimal parameters of SiC_P suspension for gelcasting process are pH value of 10, TMAH content of 0.5 wt.%, and solid loading of 52 vol.%.

(3) The alloyed matrix with Mg helps to improve the interfacial wettability and the infiltration rate. While the alloyed matrix with Si inhibits the formation of interface product Al_4C_3 effectively, and strengthens the interfacial adhesion.

(4) The obtained Al4Mg2Si/SiC_P composite exhibits a high relative density of 99.2%, good thermal conductivity of 150 $W \cdot m^{-1} \cdot K^{-1}$, low coefficient of thermal expansion of 10.1×10^{-6} K^{-1}, and excellent bending strength of 489 MPa.

References

[1] WANG Dong-mei, ZHENG Zhi-xiang, LV Jun, XU Guang-qing, ZHOU Shi-ang, TANG Wen-ming, WU Yu-cheng. Enhanced thermal conductive 3D-SiC/Al−Si−Mg interpenetrating composites fabricated by pressureless infiltration [J]. Ceramics International, 2017, 43: 1755−1761.

[2] TENG Fei, YU Kun, LUO Jie, FANG Hong-jie, SHI Chun-li, DAI Yi-long, XIONG Han-qing. Microstructures and properties of Al−50%SiC composites for electronic packaging applications [J]. Transactions of Nonferrous

Metals Society of China, 2016, 26: 2647−2652.

[3] ZHU Jian-bin, YAN Hong, YE He-yuan, AI Fan-rong. Corrosion behavior of SiC foam ceramic reinforced Al−23Si composites in NaCl solution [J]. Journal of Central South University, 2017, 24(9): 1934−1940.

[4] LI Bin, LUO Bing-hui, HE Ke-jian, ZENG Li-zhou, FAN Wen-li, BAI Zhen-hai. Effect of aging on interface characteristics of Al−Mg−Si/SiC composites [J]. Journal of Alloys and Compounds, 2015, 649: 495−499.

[5] ZHU Jing-bo, WANG Fu-chi, WANG Yang-wei, ZHANG Bo-wen, WANG Lu. Interfacial structure and stability of a co-continuous SiC/Al composite prepared by vacuum-pressure infiltration [J]. Ceramics International, 2017, 43: 6563−6570.

[6] LI Qiang, QIU Feng, DONG Bai-xin, GENG Run, LV Ming-ming, ZHAO Qing-long, Jiang Qi-chuan. Fabrication, microstructure refinement and strengthening mechanisms of nanosized SiC_P/Al composites assisted ultrasonic vibration [J]. Materials Science and Engineering A, 2018, 735: 310−317.

[7] ZHANG W Y, DU Y H, ZHANG P. Vortex-free stir casting of Al−1.5wt%Si−SiC composite [J]. Journal of Alloys and Compounds, 2019, 787: 206−215.

[8] ABOLKASSEM S A, ELKADY O A, ELSAYED A H, HUSSEIN W A, YEHYA H M. Effect of consolidation techniques on the properties of Al matrix composite reinforced with nano Ni-coated SiC [J]. Results in Physics, 2018, 9: 1102−1111.

[9] SOLTANI S, KHOSROSHAHI R A, MOUSAVIAN R A, JIANG Zheng-yi, BOOSTANI A F, BRABAZON D. Stir casting process for manufacture of Al−SiC composites [J]. Rare Metals, 2015, 36(7): 581−590.

[10] MA Y Q, QI L H, ZHOU J M, ZHANG T, LI H J. Effects of process parameters on fabrication of 2D-C_f/Al composite parts by liquid–solid extrusion following the vacuum infiltration technique [J]. Metallurgical and Materials Transactions B, 2016, 48: 1−9.

[11] WANG Dong-mei, ZHENG Zhi-xiang, LV Jun, XU Guang-qing, ZHOU Shi-ang, TANG Wen-ming, WU Yu-cheng. Multimodal particle distribution in 3D-SiC/Al−Si−Mg interpenetrating composite fabricated by pressureless infiltration [J]. Ceramics International, 2018, 44: 19851−19858.

[12] WANG Dong-mei, ZHENG Zhi-xiang, LV Jun, XU Guang-qing, ZHOU Shi-ang, TANG Wen-ming, WU Yu-cheng. Interface design in 3D-SiC/Al−Si−Mg interpenetrating composite fabricated by pressureless infiltration [J]. Ceramics International, 2018, 44: 11956−11965.

[13] REN Shu-bin, SHEN Xiao-yu, QU Xuan-hui, HE Xin-bo. Effect of Mg and Si on infiltration behavior of Al alloys pressureless infiltration into porous SiC_p preforms [J]. International Journal of Minerals, Metallurgy, and Materials, 2011, 18: 703−708.

[14] CHEN Yi-xin, WANG Ri-chu, WANG Xiao-feng, PENG Chao-qun, PENG Jian, SUN Yue-hua. Effects of Mg on microstructures and properties of SiC_p/Al composites prepared by vacuum pressure infiltration [J]. The Chinese Journal of Nonferrous Metals, 2016, 26(6): 1228−1234. (in Chinese)

[15] FALLAH-ARANI H, ISAFI S, TABRIZIAN P, MOAKHAR R S, BAGHSHAHI S. A novel gel-cast SiC with potential application in turbine hot section: Investigation of the rheological behavior and mechanical properties [J]. Ceramics International, 2019, 45: 15996−16001.

[16] KHEYRINIA L, BAHARCANDI H R, EHSANI N, YAGHOBIZADEH O. Fabrication of SiC bodies by optimized gel-casting method [J]. International Journal of Refractory Metals and Hard Materials, 2019, 81: 225−232.

[17] YANG Hong-yu, DONG Er-ting, ZHANG Bing-qi, CHEN Liang-yu, SHU Shi-li. Effects of alloying elements on the phase constitution and microstructure of in situ SiC/Al composites [J]. International Journal of Modern Physics B, 2019, 33: 1940048.

[18] LUO Z P. Crystallography of SiC/$MgAl_2O_4$/Al interfaces in a pre-oxidized SiC reinforced SiC/Al composite [J]. Acta Materialia, 2006, 54: 47−58.

[19] LEE J C, SEOK H K, LEE H I. Alloy design of thixoformable wrought SiC/Al alloy composites [J]. Materials Research Bulletin, 1999, 34: 35−42.

[20] AN Qin, CONG Xiao-shuang, SHEN Ping, JIANG Qi-chun. Roles of alloying elements in wetting of SiC by Al [J]. Journal of Alloys and Compounds, 2019, 784: 1212−1220.

[21] YI Zhong-zhou, XIE Zhi-peng, MA Jing-tao, HUANG Yong, CHENG Yi-bing. Study on gelcasting and properties of recrystallized silicon carbide [J]. Ceramics International, 2002, 28: 369−376.

[22] LI Wei, CHEN Ping, GU Ming-yuan, JIN Yan-ping. Effect of TMAH on rheological behavior of SiC aqueous suspension [J]. Journal of the European Ceramic Society, 2004, 24(14): 3679−3684.

[23] DONG Man-jiang, MAO Xiao-jian, ZHANG Zhao-quan, LIU Qian. Gelcasting of SiC using epoxy resin as gel former [J]. Ceramics International, 2009, 35: 1363−1366.

[24] QU S G, LOU H S, LI X Q, KUANG T R, LOU J Y. Effect of heat-treatment on stress relief and dimensional stability behavior of SiC_p/Al composite with high SiC content [J]. Materials and Design, 2015, 86: 508−515.

凝胶注模与真空压力浸渗法近净成形制备 Al/SiC_P 复合材料

董翠鸽[1,2]，王日初[1,2]，陈以心[1,2]，王小锋[1,2]，彭超群[1]，曾 婧[1,2]

1. 中南大学 材料科学与工程学院，长沙 410083；
2. 湖南省电子封装与先进功能材料重点实验室，长沙 410083

摘 要：针对 Al/SiC_P 复合材料机加工困难的问题，首先采用凝胶注模法得到具有复杂形状的 SiC_P 预制块，再通过真空压力浸渗近净成形制备具有高 SiC_P 体积分数的 Al/SiC_P 复合材料。复合材料基体采用三种合金，分别为纯 Al、Al4Mg 和 Al4Mg2Si。结果表明：适用于凝胶注模的 SiC_P 浆料最佳参数为 pH 10，TMAH 含量 0.5% (质量分数)和固相体积分数 52%。在 Al 基体中添加 Mg 能改善基体与 SiC_P 颗粒界面的润湿性，从而提高复合材料的相对密度；在 Al 基体中添加 Si 有助于抑制有害界面相 Al_4C_3 的生成。制备的 Al4Mg2Si/SiC_P 复合材料具有较高的相对密度(99.2%)、良好的热导率(150 $W·m^{-1}·K^{-1}$)、较低的线膨胀系数($10.1×10^{-6}$ K^{-1})以及优异的弯曲强度(489 MPa)。

关键词：Al/SiC_P 复合材料；凝胶注模；真空压力浸渗；显微组织；性能

(Edited by Bing YANG)